Hindawi
Mathematical Problems in Engineering
Volume 2021, Article ID 9640928, 14 pages
https://doi.org/10.1155/2021/9640928

Research Article

Multiobjective Optimization of an Off-Road Vehicle Suspension Parameter through a Genetic Algorithm Based on the Particle Swarm Optimization

Dengzhi Peng[1,2], **Gangfeng Tan**[1,2], **Kekui Fang**[3], **Li Chen**[4], **Philip K. Agyeman**[1,2] **and Yuxiao Zhang**[5]

[1]*Hubei Key Laboratory of Advanced Technology for Automotive Components, Wuhan University of Technology, Wuhan 430070, China*
[2]*School of Automotive Engineering, Wuhan University of Technology, Wuhan 430070, China*
[3]*Hubei Center for Quality Inspection of Special Purpose Vehicles, Suizhou 441300, China*
[4]*Dongfeng Off-road Vehicle Co. Ltd., Shiyan 442013, China*
[5]*Suizhou-WUT Industry Research Institute, Suizhou 441300, China*

Correspondence should be addressed to Gangfeng Tan; auto_nova@whut.edu.cn

Received 3 June 2020; Revised 27 December 2020; Accepted 11 January 2021; Published 1 February 2021

Academic Editor: Mahmoud Mesbah

Ride comfort and handling performances are known conflicts for off-road vehicles. Recent publications focus on passenger vehicles on class B and class C roads, while, for off-road vehicles, they should be able to run on rougher roads: class D, class E, or class F roads. In this paper, a quarter vehicle model with nonlinear damping is established to analyze the suspension performance of a medium off-road vehicle on the class F road. The ride comfort, road holding, and handling performance of the vehicle are indicated by the weighted root mean square (RMS) value of the vertical acceleration of the sprung mass, suspension travel, and tire deflection. To optimize these objectives, the genetic algorithm (GA), particle swarm optimization (PSO), and a genetic algorithm based on the particle swarm optimization (GA-PSO) are initiated. The efficiency and accuracy of these algorithms are compared to find the best suspension parameters. The effect of the optimized method is validated by the field test result. The ride comfort, road holding, and handling performance are improved by approximately 20%.

1. Introduction

The suspension system of a vehicle is a vital assembly and it is crucial to the ride comfort, handling stability, and safety of the car. However, the ride comfort conflicts with handling stability; in a literal term, a better ride comfort means worse handling stability, and vice versa. Hence, to improve vehicle performance, some optimization algorithms are used to modify the suspension parameters. Recent research focuses on the passenger vehicle because it has more consumers, and its vehicle performance has a direct impact on its consumption. Liu et al. modified some parameters of the suspension to reduce the vibration caused by the in-wheel motor [1]. The improved particle swarm optimization (IPSO) is used to determine the spring stiffness. Kanarachos et al. provided a new enhanced fruit fly optimization (eFLO) algorithm to improve the suspension shock without degrading road holding and ride comfort [2]. In their research, the optimization algorithm, differential evolution (DE), artificial bee colony (ABC), and particle swarm optimization (PSO) are taken as benchmarks, and a class C road was used in the simulation. Yang proposed an improved genetic algorithm based on fitness evaluation to analyze the ride comfort of an in-wheel motor vehicle on the class B road; the RMS value of the vehicle weighted vertical acceleration and the pitching angle acceleration are taken as the objectives [3]. The PSO is initiated in Li's research [4] and an improved GA named KEMOGA is provided [5] to

optimize the ride comfort of the passenger vehicle on class B and class C roads. They all take the RMS of the weight vertical acceleration, suspension travel, and tire deflection as their objectives. In these researches, passive suspension and optimizing the suspension parameters can improve the objectives by 5~15%. Besides the traditional suspension which suppresses the vibration, the regenerative suspension that focuses on harvesting the vibration energy of the suspension system also attracts the researchers' attention [6]; Abdelkareem et al. acquired the energy that dissipated of an SUV on class B road [7] and designed regenerative shock absorbers to harvest the energy [8].

According to the ISO/TC108/SC2N67, roads can be classified as classes B, C, D, E, and F by the road roughness coefficient. The road roughness coefficient increases from class B to class F, which means the class F road is the roughest. The passenger vehicle usually runs on class B to class D roads; off-road vehicles are capable of running on class E and class F roads. Semiactive and passive suspension systems are used for off-road vehicles on class F roads, which provide an improved vehicle performance of 20~40%, but their reliability still needs to be verified [9]. Ghasemiazar and Azadi purported an improved off-road vehicle performance (17% during the simulation) by the design of experiment (DOE) and response surface method (RSM) [10].

The damper is taken as a linear parameter when the vehicle runs on an urban road, while, on rough roads, the nonlinear characteristic of damping should be taken into consideration. Xudong et al. proved that the suspension with nonlinear damping has better anti-impact performance than the suspension with linear damping [11]. Zhao et al. analyzed the seat suspension system considering the nonlinear characteristic; the result is validated by an experimental test rig [12]. Nonlinear damping also allows the vehicle to have a better adaptation to different road surfaces. Solomon and Padmanabhan developed a semiactive suspension with nonlinear damping to improve the ride comfort performance without compromising the road holding and load carrying of the vehicle [13]. Zhang et al. improved the mine car ride comfort on class C road based on the improved particle swarm optimization and approximation model [14]. Sun proposed a new algorithm based on cuckoo search (CS) optimization and road estimation to investigate the characteristics of the nonlinear parameters and improve ride comfort [15]. Mahmoodi-Kaleibar optimized a suspension system of an off-road vehicle with the curb weight of 1800 kg according to optimized GA [16].

Most of the current researches validate the optimization by simulations, and some of them use a test rig to verify the result. The research about the mid-sized off-road vehicle on the class F road is rare.

In this paper, the approximation model of the vehicle performance indicators and the suspension parameter of a mid-sized off-road vehicle are established according to the RSM. Three multiobjective optimization methods are initiated and compared to gain the best solution for the vehicle suspension system. At last, the optimization is validated by the field test. Figure 1 shows the flow chart illustration described in this paper. Compared to the passenger car on class B and class C roads, the optimization of the off-road vehicle can improve the vehicle performance with a higher percentage. The optimized suspension parameters can not only be useful to the design of passive suspension but also be used in the semiactive or active suspension system to improve vehicle performance.

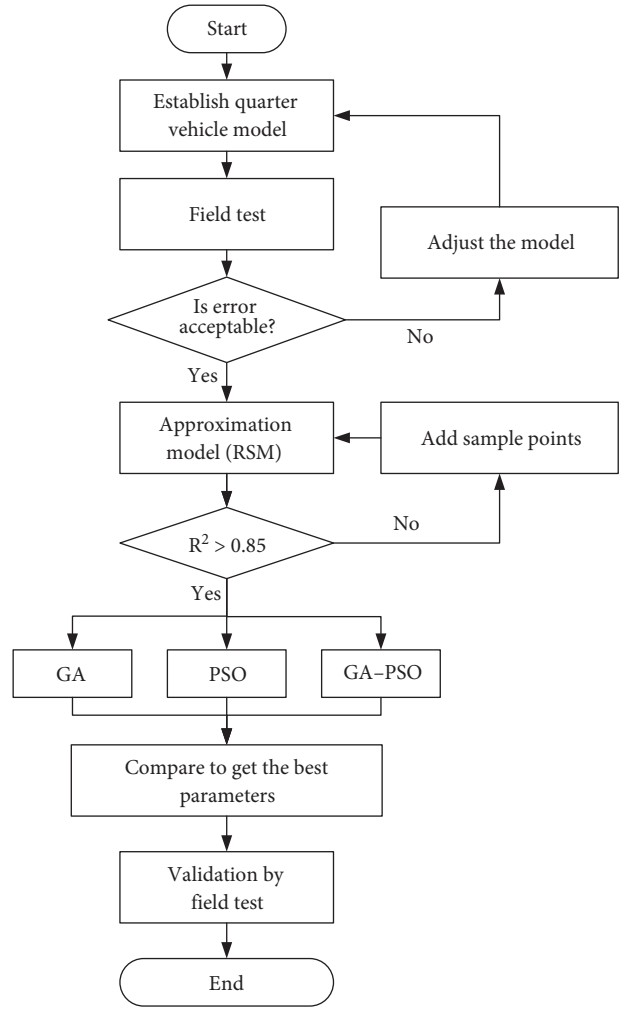

Figure 1: Flow chart of the work. A nonlinear model of the quarter vehicle.

The quarter vehicle mathematical model is used in vehicle performance analysis due to its efficiency [17, 18]. As shown in Figure 2, which shows the classic quarter vehicle model, the tire is modeled as a linear spring (K_t), which is a fundamental representation of tires. In practice, vehicle ride combines with tire characteristics that alter vehicle bounce and particularly pitch dynamics. In this paper, very basic tire behavior is assumed. For more representative tire behavior, affecting pitch-plane dynamics, see Abdelkareem et al. [19]. The tire receives the input of the road surface in the time domain, $q(t)$. The suspension, which connects the unsprung mass (m_1) with the sprung mass (m_2), consists of linear spring (K) and nonlinear damping (C). Equation (1) is the governing equation of this model. z_1 and z_2 are the displacements of the unsprung mass and sprung mass, respectively.

$$\{m_2\ddot{z}_2 + C(\dot{z}_2 - \dot{z}_1) + K(z_2 - z_1) = 0, m_2\ddot{z}_1 + C(\dot{z}_1 - \dot{z}_2) + K(z_1 - z_2) + K_t z_1 = q(t). \quad (1)$$

The damping force during the compression and the stretching process is different, and the nonlinear relationship is the damping force and velocity. The nonlinear damping characteristic can be described by a piecewise function, shown in equation (2). In this equation, F_c is the damping force, v_c and v_s are the velocities during the compression and stretching process, respectively, and c_{c1}, c_{c2}, and c_s are the corresponding damping values.

$$F_c = \begin{cases} c_{c2}(v_c - v_{c1}) + c_{c1}v_{c1}; & v_{c2} \le v_c, \\ c_{c1}v_c; & \\ c_s v_s; & v_{c1} \le v_c \le 0. \end{cases} \quad (2)$$

According to the harmonized superposition method, the random road surface can be described as follows:

$$\dot{q}(t) = -2\pi f_0 x_z(t) + 2\pi\sqrt{G_0 v}\, w(t), \quad (3)$$

where G_0 is the road roughness coefficient, v is the vehicle velocity, w is the Gaussian white noise with zero mean value, and f_0 is the lower stopband edge frequency.

This quarter vehicle model with a nonlinear damping and random input road can be simulated by MATLAB/Simulink, as Figure 3 shows. The parameters of this simulation model are shown in Table 1.

The suspension system is capable of isolating the vehicle body (sprung mass) from road roughness and provides the passengers and cargo good ride quality. When the vehicle is simplified as a quarter model, the ride comfort can be quantified by the vertical acceleration of the sprung mass ($\ddot{z}_2$). According to the ISO-2631 standard, which evaluates human exposure to whole-body vibration, the ride comfort could be measured via the weighted RMS acceleration (A_w).

$$A_w = \left\{\int_{0.5}^{80} \left[W^2(f)G_a(f)\right]^2 \mathrm{d}f\right\}^{(1/2)}, \quad (4)$$

where $G_a(f)$ is the power density function of $\ddot{z}_2$, which can be gained through FFT (fast Fourier transform), $W(f)$ is the weight factor function, and f is the frequency.

The suspension travel is taken as the indicator to measure the ability to support the static weight of the vehicle. The tire deflection, which is relevant to the normal tire force, illustrates the road holding and the vehicle handling performance. The RMS suspension travel, s_t, and RMS tire deflection, t_d, can be acquired by equations (5) and (6). $F_t(t)$ is the tire load and acts as a function of time.

$$s_t = \left\{\frac{1}{T}\int_0^T [z_2 - z_1]^2 \mathrm{d}t\right\}^{(1/2)}, \quad (5)$$

$$t_d = \left\{\frac{1}{T}\int_0^T \left[\frac{F_t(t)}{K_t}\right]^2 \mathrm{d}t\right\}^{(1/2)}. \quad (6)$$

2. Field Test and Model Validation

To verify the effect of the quarter vehicle model, the field test on the class F road is carried out in the Dingyuan test field. The gross vehicle mass of the vehicle is 5300 kg and the tire of the front and rear axle is 335/80 R20. The structures of the front and rear suspensions are similar; both of them have a double wishbone, coil spring, and damper. The front suspension is equipped with an antiroll bar, while the stabilizer bar is mounted on the rear suspension. During the test, two acceleration sensors are mounted on the lower suspension arm and the upper spring mount seat, a seat acceleration sensor is mounted on the driver's seat, and a speed sensor and a data acquisition system are equipped to collect the data as shown in Figure 4. The off-road test field is illustrated in Figure 5. The details of the sensors in the test are shown in Table 2. Since the parameters of the quarter vehicle are the equivalent value of the rear suspension, the sensors are mounted on the rear right suspension.

During the test, the vehicle runs in the field with a speed of 15 km/h, the sampling frequency of the acceleration is 200 Hz, and the speed sensor is 20 Hz. To avoid high-frequency interference and energy leakage, the Hanning window is used to process the signals. The cut frequency of the Hanning window is set as 100 Hz to ensure the reliability of the results.

The tested and simulated acceleration signals on the upper suspension mount and lower arm are shown in Figures 6 and 7.

As shown in Figures 6 and 7, the trends of the test and simulated accelerations are similar to each other. The weighted RMS of the upper mount acceleration (body acceleration in the quarter vehicle model) and the RMS of the lower arm acceleration (wheel acceleration in the quarter vehicle model) are calculated. For the upper mount, the weight RMS accelerations of the test and simulation are 3.36 and 3.22 m/s^2; for the lower arm, the RMS accelerations of the test and simulation are 34.91 and 38.76 m/s^2. The errors between the test and the simulated results are −4.17 and 11.03%, respectively. The error of the lower arm acceleration is caused by taking the tire as a linear spring model. Since the errors are in a relatively low range, the quarter vehicle model can be used in further analysis.

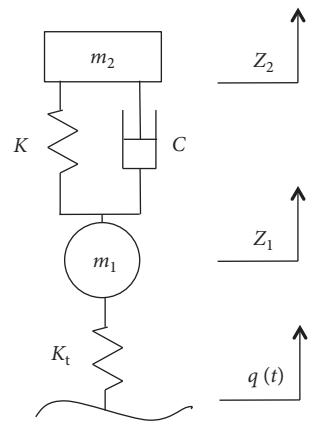

Figure 2: A quarter vehicle model.

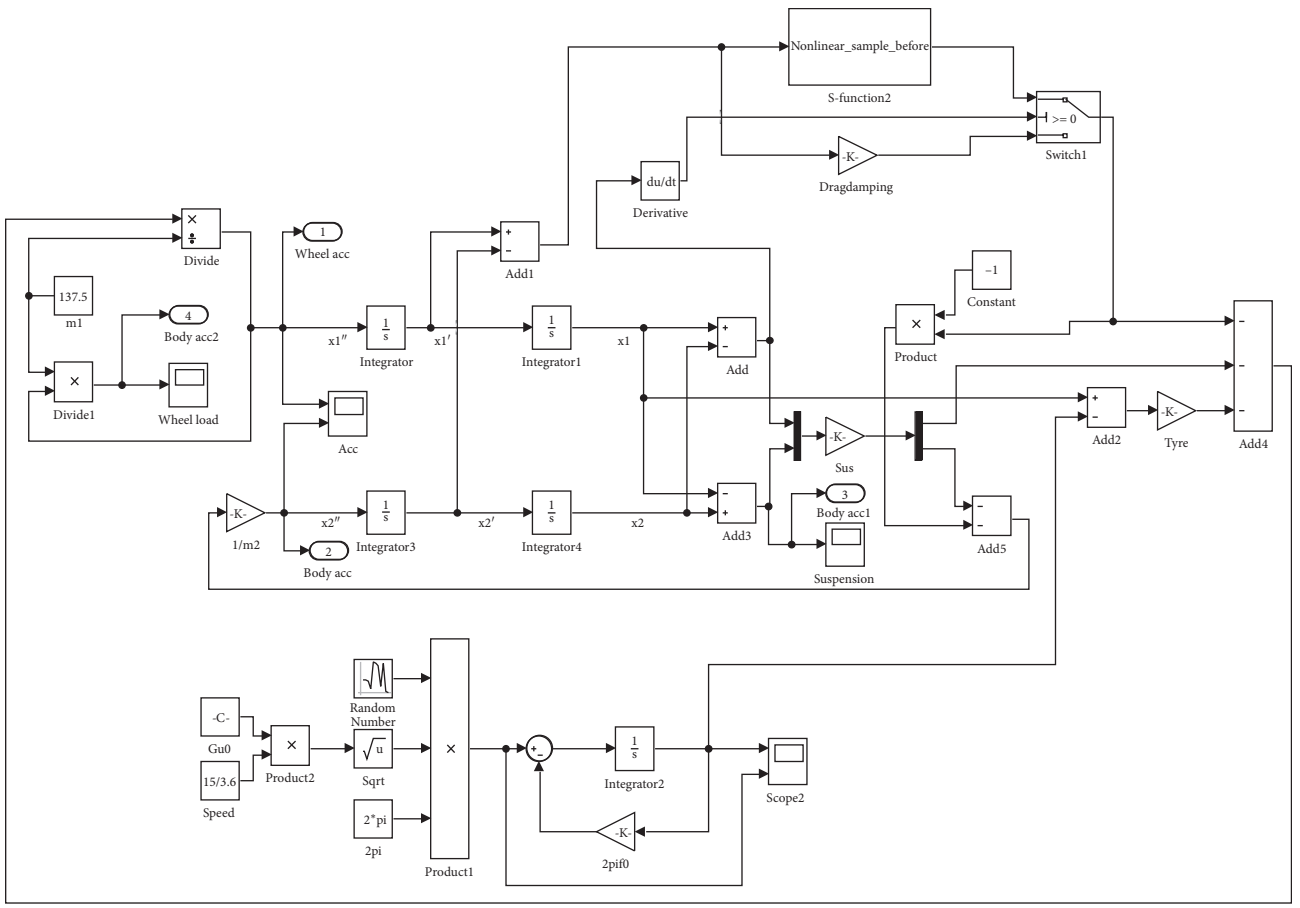

Figure 3: A quarter vehicle model with a random road.

Table 1: Parameters of the simulation model.

Vehicle parameters			
m_2 (kg)	137.5	K_t (N/m)	205000
m_1 (kg)	1262.5	K (N/m)	56000
c_s (N·s/m)	9600	c_{c1}/c_{c2} (N·s/m)	4800/1200
Road parameters			
G_0 (m^3)	0.016384	f_0 (Hz)	0.1

3. Establishment of the Approximation Model

The approximation model of these three objectives of the suspension parameters can be established through the response surface method (RSM); the validity of this method has been validated by [20, 21]. The approximation model can also reduce the optimization time. Taking the tire stiffness K_t, spring stiffness K, compression dampings c_{c1} and c_{c2}, and stretch damping c_s as the factors, three functions have been established as follows:

$$\begin{aligned} A_w = {} & 4.83 + 2.1e^{-5}K_t - 2.51e^{-4}K + 2.65e^{-4}c_s + 4.4e^{-5}c_{c1} - 5.9e^{-5}c_{c2} + 1.61e^{-9}Kc_{c2} \\ & + 2.09e^{-9}c_sc_{c1} + 8.66e^{-9}c_sc_{c2} + 1.54e^{-8}c_{c1}c_{c2} + 2.29e^{-9}K^2 - 9.42e^{-9}c_{c1}^2 \\ & - 1.24e^{-8}c_{c2}^2, \end{aligned} \tag{7}$$

$$\begin{aligned} s_t = {} & 12.57 + 2e^{-5}K_t - 6.55e^{-4}K + 3.45e^{-4}c_s + 6.66e^{-5}c_{c1} - 5.9e^{-5}c_{c2} \\ & - 1.66e^{-9}c_{c1}c_{c2} + 5.06e^{-9}K^2 - 1.69e^{-8}c_{c1}^2 - 2.98e^{-8}c_{c1}^2 - 1.16e^{-7}c_{c2}^2, \end{aligned} \tag{8}$$

$$t_d = 6.39e^{-2} - 9.26e^{-8}K_t - 1.03e^{-9}K - 8.11e^{-8}c_s - 8.07e^{-6}c_{c1} - 5.9e^{-5}c_{c2} + +5.81e^{-10}c_{c2}^2. \tag{9}$$

The coefficient of determination, R^2, is used for its validation check. R^2 means the similarity between the predicted value and the sample value, the closer to 1, means the higher accuracy of the prediction equation is. It can be generated by the following equation:

$$R^2 = 1 - \frac{\sum_{i=1}^{n}\left(T_i - \widehat{T}_i\right)^2}{\sum_{i=1}^{n}\left(T_i - \overline{T}\right)^2}, \tag{10}$$

where T_i is the value of sample i and $\widehat{T}_i$ is the predicted value based on sample i. The number of the samples is n and $\overline{T}$ is the mean value of n samples.

In this case, R^2 of equations (7), (8), and (9) are 0.87, 0.86, and 0.93, respectively.

As can be seen in Figures 8–10, despite a singular point, most of the data points in these figures are approximately linear. Therefore, these functions can be used for further analysis.

4. Optimization Algorithms

4.1. Genetic Algorithm (GA). GA is an optimization problem-solving method that is inspired by natural selection. The idea of this algorithm is to adapt a population to environmental conditions like what happens to genes in nature [22]. Each individual of the population has its characteristic; in the optimization process, the effective traits are improved, while the undesired characteristics are eliminated. In each iteration, new populations are generated by selection, crossover, and mutation. In the selection stage, the first generation of the population or the individuals with good traits from the last generation is chosen to be the new parents to start a new loop. The crossover is the process of two individuals (parents) producing new individuals (children). The mutation stage is a random change in one gene of the new individuals (children) from its initial state, which is inherent from their parents. The iteration keeps process until the object meets the fitness or the iteration limits to find the optimized value of the factors.

In the multiobjective genetic algorithm process, the whole population is checked, and the nondominated individuals are identified and assigned with dummy fitness. Then the individuals are selected based on dummy fitness. The following crossover and mutation processes are the same as the classic GA method.

4.2. Particle Swarm Optimization (PSO). PSO algorithm is a population-based stochastic approach that uses the velocity and a position search model, including a certain number of particles that are used to represent candidates; the position of each particle is used to represent a solution of space, and the velocity is used to update the particle position [23]. Each particle searches for better positions in the search space according to its local best position and global best position [24]. At the beginning, the particle's velocity and position are arbitrarily assigned in a proposed range. Then, the particle's velocity v_k and position x_k can be improved via the following equations:

$$v_k(i+1) = w(i) \times v_k(i) + c_1 \times r_1\left(\text{pbest}_k(i) - x_k(i)\right) + c_2 \times r_2\left(\text{gbest}(i) - x_k(i)\right), \tag{11}$$

$$x_k(i+1) = v_k(i+1) + x_k(i), \tag{12}$$

where k is the particle's index, ranging from 1 to N_p, N_p is the population of the particle, i is the iteration number, ranging from 1 to $i_{\max}$, r_1 and r_2 are two numbers that are generated randomly between 0 and 1, c_1 and c_2 are

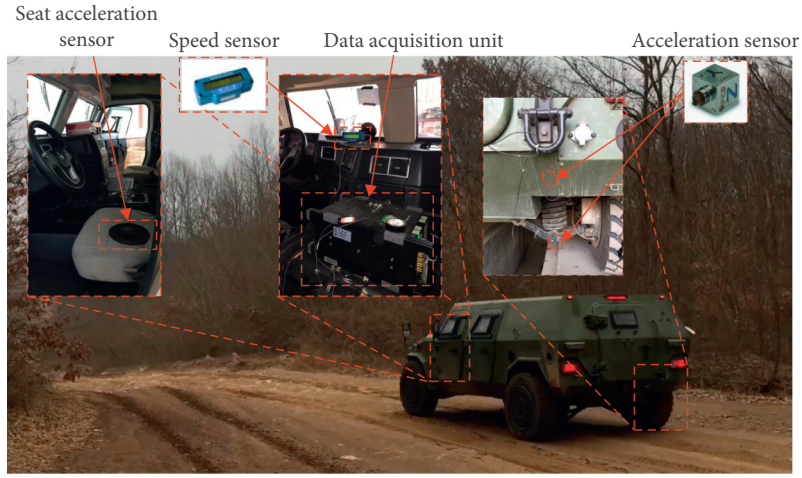

Figure 4: Sensors and data acquisition unit on the tested vehicle.

Figure 5: Test field.

learning factors, pbest is the best experience of each particle, and gbest is the best experience of all particles in the population. The position and value of the objective function for pbest and gbest must be stored after each iteration. The iteration begins after the initial evaluation if the termination criterion is satisfied, the optimal solution reaches gbest, and the calculation is ended; otherwise, the iteration repeats.

For the multiobjective problem, the optimal solutions are called the Pareto solution. In the multiobjective particle swarm optimization process, each particle of the population should select one of the Pareto solutions as its global best particle, called the best local guide. The analysis of the sigma method provided by Mostaghim is used in this paper [25]. According to the sigma method, the fitness of the particles is calculated and ranked before the next iteration.

4.3. GA-PSO Algorithm. Although GA is one of the most popular methods for solving the multiobjective problem, its main disadvantage is the low convergence rate. PSO has a quicker convergence, but its limitation is easy to get stuck in local extremes [26]. To overcome its weakness, the hybrid GA-PSO algorithm is provided by [27]. As shown in Figure 11, this algorithm begins with a main iterative loop, which has a stop criterion of max_it to show the iterations of the whole algorithm. After that, the PSO loop gets started. In PSO iteration, the fitness of each particle is evaluated and the particles' best is chosen; then the specific particle assigned to that would be the best experience of that particle (pbest). Then the global best position (gbest) will be acquired. For the next stage, the position and velocity of each particle are updated according to equations (11) and (12).

The particles prepare to be acted in GA iteration after the first loop ends. For the first operator in GA, two random particles are selected and updated using the following equations, if the probability condition is met.

$$\begin{aligned} x_1(i+1) &= \alpha x_1(i) + (1-\alpha)x_2(i), \\ x_2(i+1) &= \alpha x_2(i) + (1-\alpha)x_1(i). \end{aligned} \tag{13}$$

The above equations represent the crossover stage in GA, $\alpha \in [0,1]^D$ is a random vector, and D is the dimension size, which could be the factor's size in the proposed method.

In the mutations stage, the particle mutates via the following equation, if the mutation probability condition is satisfied.

$$x(i+1) = x(i) + \text{randn} \times \sigma, \tag{14}$$

$$\sigma = \frac{(\text{maximum domain} - \text{minimum domain})}{10}, \tag{15}$$

where randn is a normal random integer and σ is a constant value generated by equation (15).

The crossover and mutation had been modified regarding obtaining better results than the original GA [28]. At last, the algorithm checks for the updates of pbest for each particle and gbest for the whole particles.

Table 2: Details of the sensor in the field test.

No.	Sensor	Type	Sampling frequency (Hz)
1	Acceleration sensor	PCB 356A45	0.4~1000
2	Seat acceleration sensor	PCB 356B40	0.5~1000
3	Speed sensor	V-box speed sensor range	5/10/20/100
4	Data acquisition unit	B&K LAN-XI	

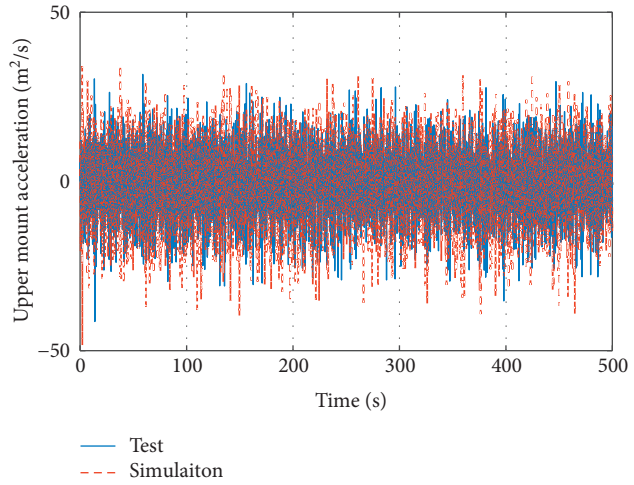

Figure 6: Comparison of the acceleration at the suspension upper mount.

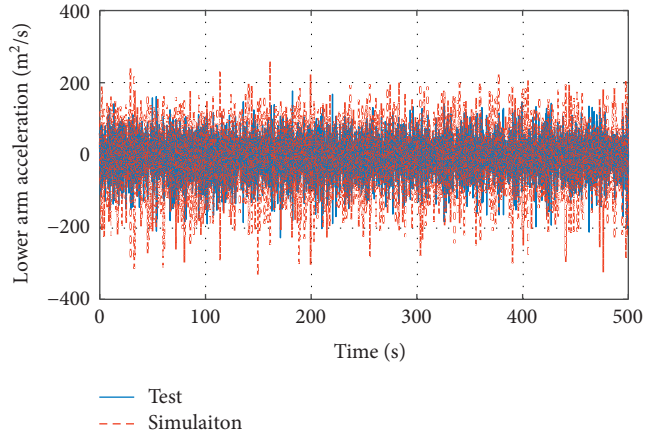

Figure 7: Comparison of the acceleration at the suspension lower arm.

5. Simulation Result and Discussion

To identify the performances of these three algorithms in terms of accuracy and efficiency, they are applied to estimate the best parameters of the quarter model. In the process of optimization, the population sizes of the algorithms are set in the range from 5 to 800, and the iteration number is 1000. The computation time and fitting value are listed in Table 3.

To illustrate the differences between the above methods, Figure 12 further displays the fitness value of them. The fitness value of GA sharply drops from 3.637 to 2.191 at the population size of 400, while the fitness value of PSO is almost stable at the population size of 600. For the GA-PSO, the fitness value seems to be stable with a value of 2.178 at the population size of 50. Since the computation time of GA-PSO is far larger than those of the other two algorithms, only GA and PSO are compared in Figure 13. The computation times of GA and PSO are close to each other when the population size is lower than 200; after that size, the GA takes about 10~20% longer computation time than the PSO. Taking the fitness value into consideration, the fitness value of the GA is stable at the population size of 400, and the corresponding computation time is 8.128 s; for the PSO, the computation time is 8.52 s at the population size of 600; for GA-PSO, the time is 12.433 s at the size of 50. GA-PSO converges at a lower population with a longer computation time due to the more complicated process.

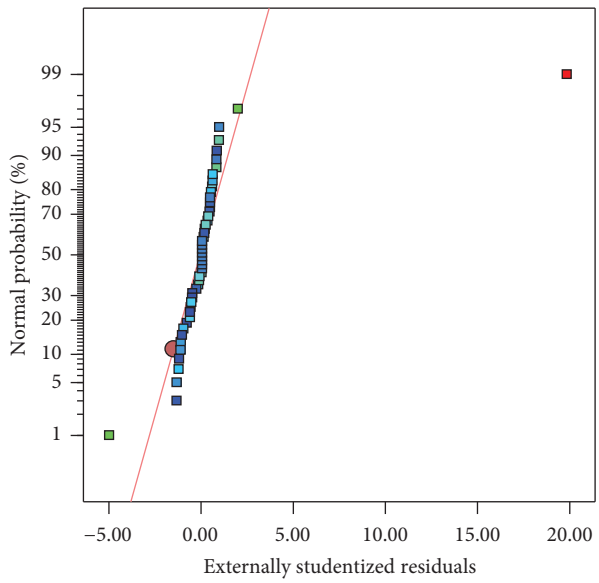

Figure 8: The normal plot of residuals of weight RMS acceleration.

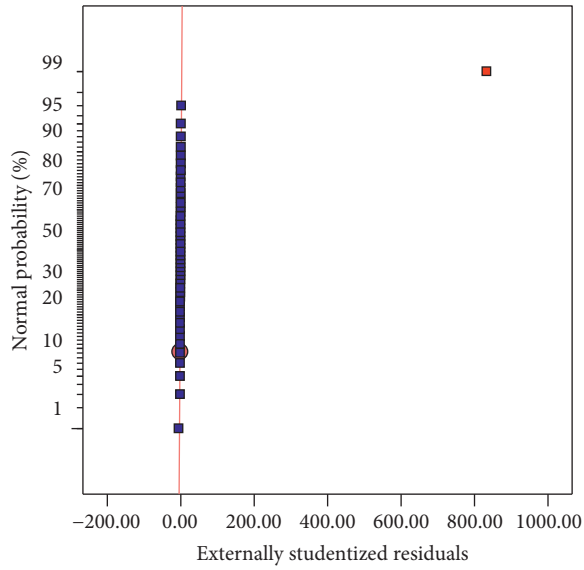

Figure 9: The normal plot of residuals of RMS suspension travel.

The search range of the parameters is shown in Table 4. The minimum stiffness and maximum stiffness of the tire are taken as the search range. For the damping coefficient of the damper, 50% and 200% of the original values are taken as search limits. The search range of the stiffness of the spring is set to 31000 to 81000 N/m based on the advice of the component manufacturers. The objectives are constrained as higher than 85% of the original value.

The population size is set as 600, the iteration generation as 1000 in the three algorithms, the crossover operator as 0.7, and the mutation operator as 0.3 in the GA. The learning factor is taken as 1.5 in the PSO. In GA-PSO, the operators and learning factors are set the same as in the GA and PSO. The Pareto solutions are gained and shown in Figures 14–16, respectively.

Taking the solution with a lower value of the three objects as the solution in the Pareto solutions (the red dot in the solutions), the corresponding optimized parameters are shown in Table 4. To validate the effectiveness of them, these parameters are set in the quarter vehicle model to generate the objectives at speeds of 5, 10, 15, 20, and 25 km/h, and the figures are shown below.

All the optimized parameters have improved the objectives compared to the original values (Figures 17–19).

For A_w, the optimized results acquired by GA and GA-PSO methods are similar and better than those of the PSO method and the original. For s_t, the optimized parameters gained by PSO are similar to those gained by GA-PSO, which are lower than the others. For t_f, the PSO and GA have lower values than those in the GA-PSO at 5 km/h; the result gained by GA-PSO has the lowest value when the speed is within 10 to 25 km/h.

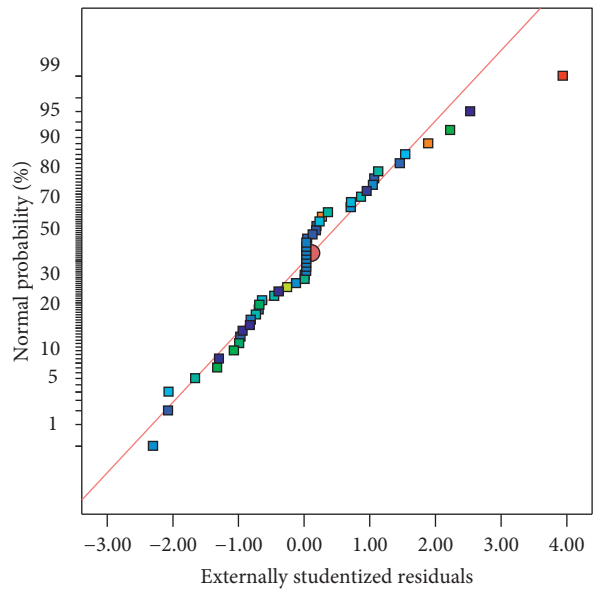

Figure 10: The normal plot of residuals of RMS tire deflection.

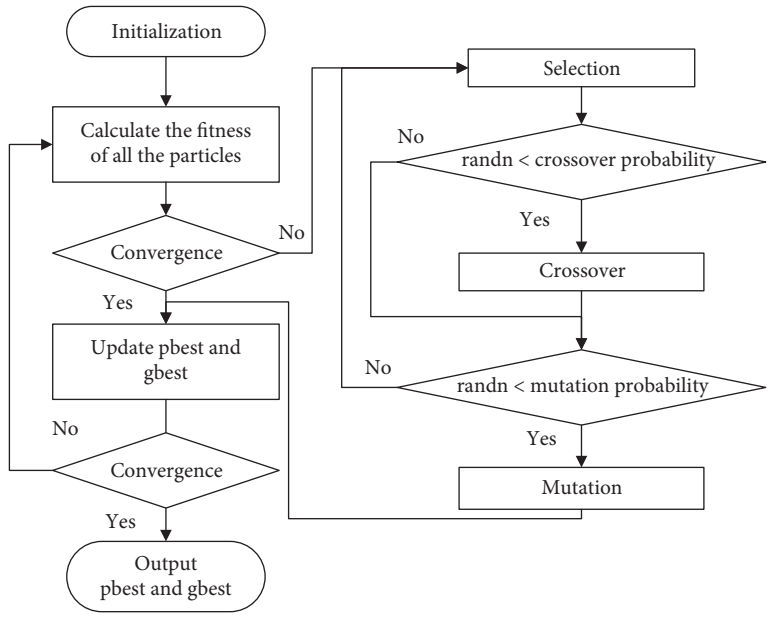

Figure 11: Flow chart of the GA-PSO algorithm.

Table 3: Computation time and fitting value of GA, PSO, and GA-PSO.

Population size	GA		PSO		GA-PSO	
	Time (s)	Fitness	Time (s)	Fitness	Time (s)	Fitness
5	0.801	3.637	0.534	2.443	0.851	2.179
25	0.958	2.673	0.545	2.243	3.898	2.179
50	1.196	3.367	0.926	2.307	12.433	2.178
100	1.600	2.432	1.892	2.243	43.346	2.178
200	2.559	2.294	2.236	2.243	164.688	2.178
400	8.128	2.191	6.119	3.307	1033.632	2.178
600	10.106	2.190	8.520	2.243	3673.503	2.178
800	12.849	2.193	11.447	2.243	8033.114	2.178

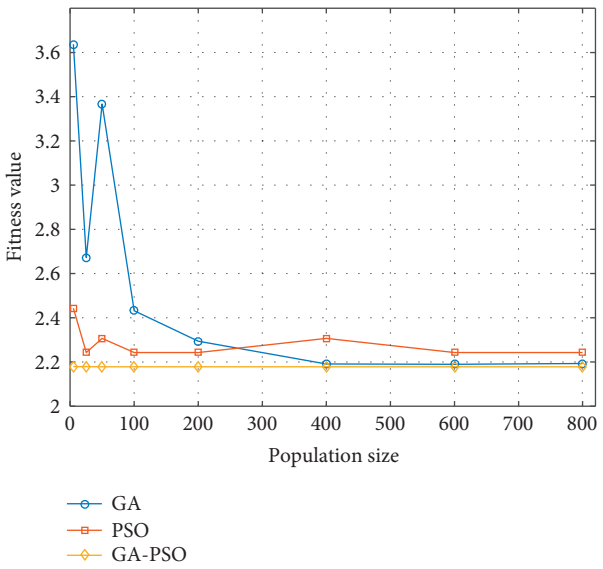

Figure 12: Comparison of the fitness values of PSO, GA, and GA-PSO.

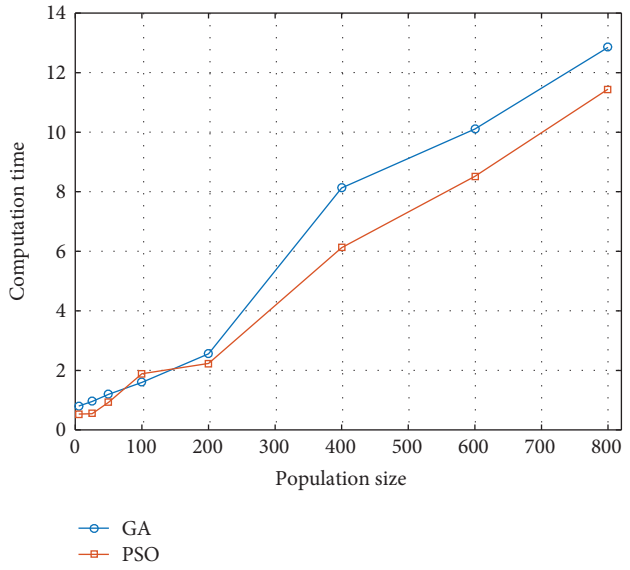

Figure 13: Comparison of PSO and GA's computation times.

Table 4: Search range and optimized value of the parameters in GA, PSO, and GA-PSO.

Parameters	Search range	Optimized value		
		GA	PSO	GA-PSO
K_t (N/m)	[205000, 435000]	217218.01	205000	225901.19
K (N/m)	[31000, 81000]	52035.0	61932	56612.8
c_s (N.s/m)	[4800, 19200]	6094.30	4800	5668.45
c_{c1} (N.s/m)	[2400, 9600]	7670.64	2400	6966.20
c_{c2} (N.s/m)	[1200, 4800]	3088.93	4800	3724.31

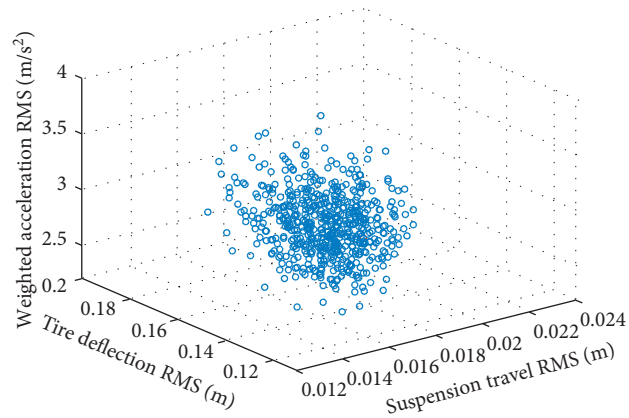

Figure 14: Pareto solutions of GA.

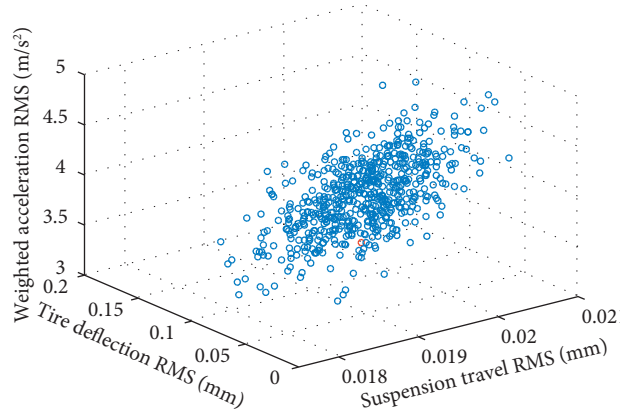

Figure 15: Pareto solutions of PSO.

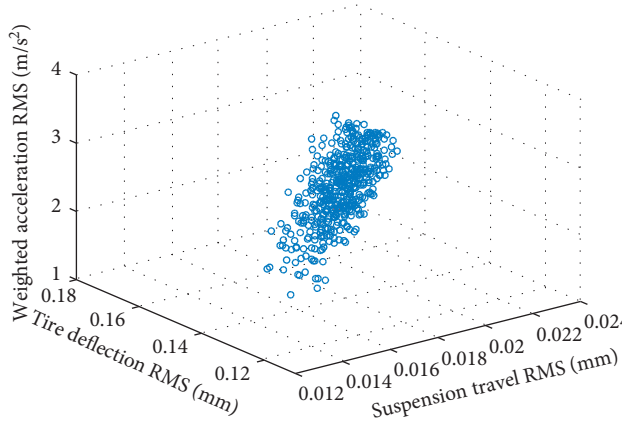

Figure 16: Pareto solutions of GA-PSO.

In general, the GA-PSO method has the lowest optimized objectives; hence, the average optimized percentages of the three objectives (A_w, s_t, and t_f) by GA are 8.41, 17.04, and 14.38%, and, for the PSO, the percentages are 3.14, 22.61, and

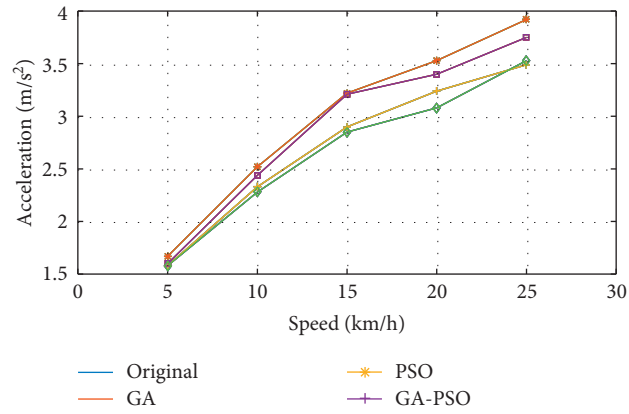

Figure 17: Weighted RMS acceleration at a different speed.

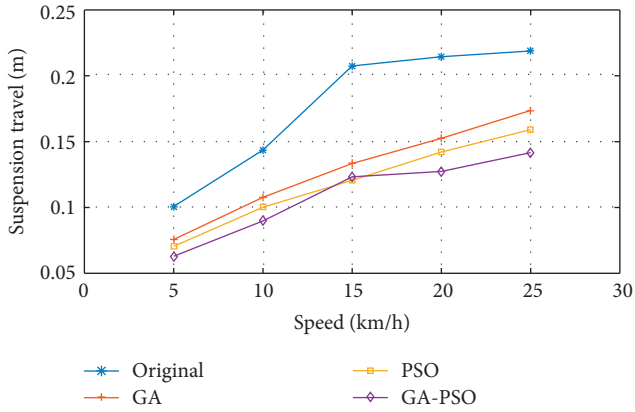

Figure 18: RMS suspension travel at a different speed.

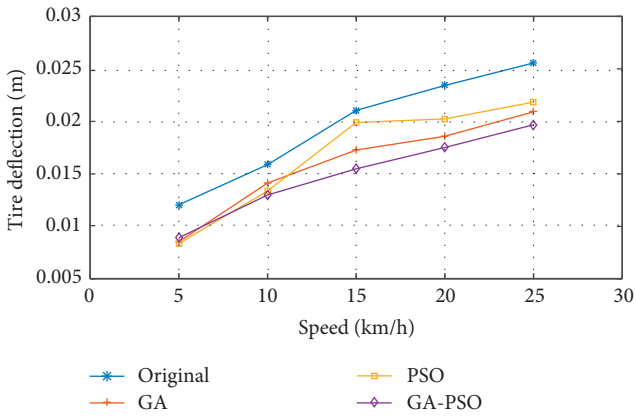

Figure 19: RMS tire deflection at a different speed.

12.00%. The corresponding percentages of the GA-PSO are 9.82, 28.29, and 18.79%. Therefore, the parameters gained by GA-PSO are used to improve the suspension system.

6. Comparison of the Test before and after Optimization

The vehicle with the optimized suspension parameters is used to conduct the field again in the same test field in "Field Test and Model Validation." Only the vehicles with GA-PSO optimized suspension parameters and original parameters are tested in the field test. The test result of the two experiments is marked as after optimization and before optimization, respectively.

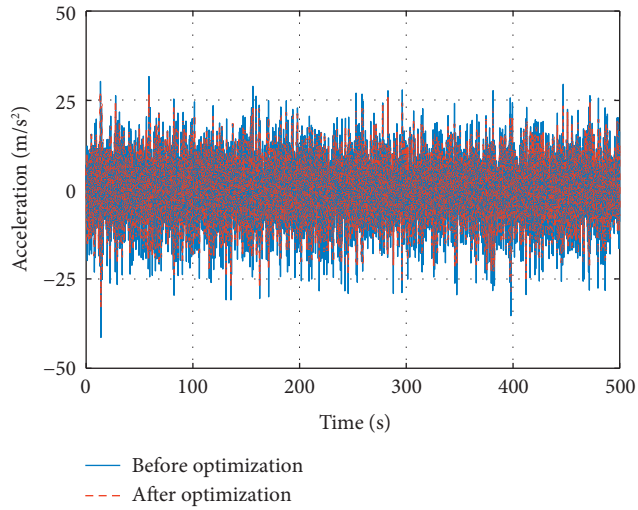

Figure 20: Comparison of acceleration before and after optimization.

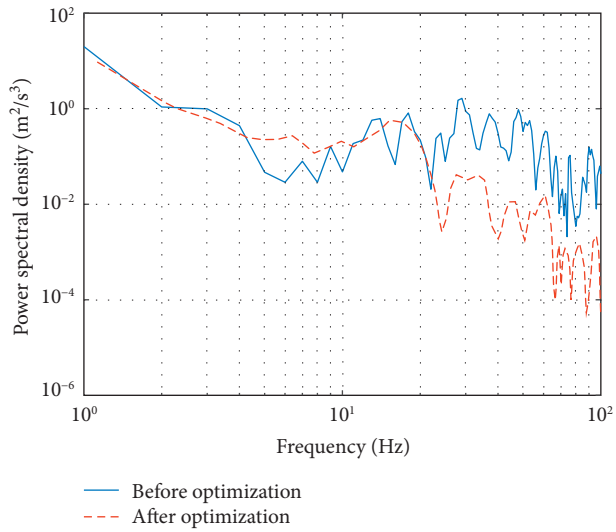

Figure 21: Comparison of vertical acceleration weighted PSD.

The vertical accelerations at the upper spring seat before and after optimization are compared in Figure 20. The power spectral density (PSD) curves of the vertical acceleration are shown in Figure 21.

According to Figure 21, the frequency is in the ranges of 0~4 and 8~20 Hz; for the PSD of vertical acceleration, the vehicle with optimized parameters is similar to the vehicle before optimization. The vertical acceleration PSD after optimization is lower than that before the optimization of 4~8 Hz. In the frequency range of 20~100 Hz, the vertical acceleration PSD of the vehicle with optimized parameters is much lower than that of the vehicle with parameters before optimization. Even though in the human sensitive frequency

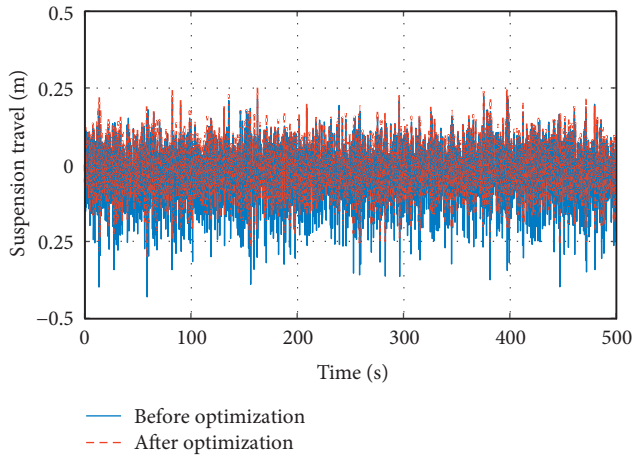

Figure 22: Comparison of suspension travel before and after optimization.

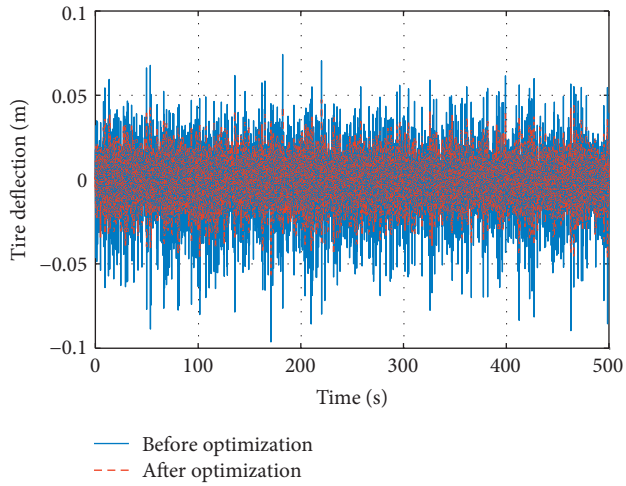

Figure 23: Comparison of tire deflection before and after optimization.

range of 4 to 8 Hz the PSD after optimization is lower than that before optimization, the acceleration weighted RMS after optimization is higher than that before optimization; thus, the ride comfort after optimization is improved.

The suspension travel and tire deflection curves are calculated based on the acceleration signals and shown in Figures 22 and 23.

In Figures 22 and 23, the suspension travel and tire deflection of the vehicle with parameters after optimization are lower than those of the vehicle with parameters before optimization. For the tire deflection, the negative value means that the wheel is not in contact with the road surface at that time.

The weighted RMS acceleration of the seat, A_{ww}, is gained based on the data acquired by the seat acceleration sensor. To compare these values more intuitively, the acceleration weighted RMS and RMS of the suspension travel and tire deflection are calculated and compared in Table 5.

After the parameter optimization, the RMS values of the vertical weighted acceleration, suspension travel, tire deflection, and RMS acceleration on the seat are improved by 18.24, 21.95, 21.34, and 15.19%, respectively. The ride comfort, road holding, and handling performance of the vehicle are substantially improved.

There are some vibration assessment methods in ISO 2631 : 1 [29]. According to Annex B, the health guidance caution zones as shown in Figure 24 are used to access the vibration exposure time. In Figure 24, the zone is determined by two dashed lines. For the exposures below the lower line, health effects have not been clearly documented or observed; in the zone, caution concerning potential health risks is indicated and above the upper line health risks are likely.

The seat acceleration RMS before (blue dot) and after (red dot) optimization is added in Figure 24. The exposure duration after optimization is 25 min, while the time duration before the optimization is 16 mins. The duration time is improved by 56.25%.

According to Annex C, the acceleration translated to the human body greater than 2 m/s^2 causes extreme discomfort. The weighted acceleration before and after optimization lies

Table 5: Comparison of objectives before and after optimization.

Objective	Before optimization	After optimization	Improvement rate (%)
A_w (m/s^2)	3.36	2.74	18.46
s_t (mm)	157.2	122.7	21.95
t_f (mm)	14.01	11.02	21.34
A_{ww} (m/s^2)	2.67	2.31	15.19

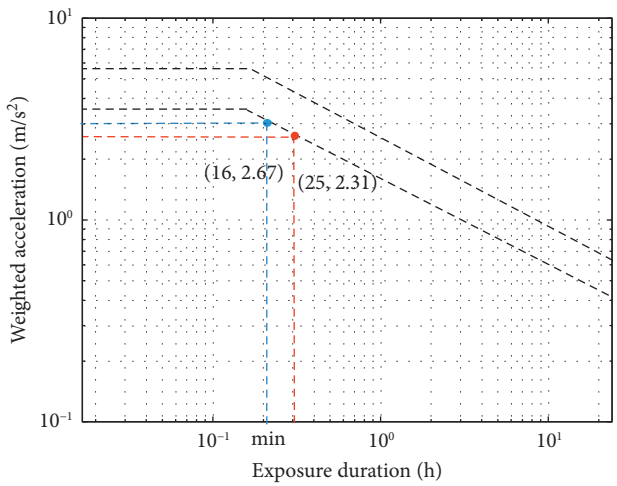

Figure 24: Health guidance caution zones in ISO 2631-1.

in this range. Because the roughness of the class F road is hard to overcome, a lower acceleration after optimization still improves the vehicle ride comfort.

7. Conclusion

To improve the performance of a military off-road vehicle on the class F road, three multiobjective optimization algorithms are initiated based on a quarter vehicle model. The ride comfort, road holding, and handling performance of the vehicle are chosen as the objectives, while some suspension parameters are taken as the variables. Three approximation models are built by RSM to establish the relationships between them. By comparing the results of GA, PSO, and GA-PSO, GA-PSO represents the closest convergence solution to the global optimum, while the GA represents the quickest convergence to the solution.

Furthermore, based on the optimized parameters, the weight RMS acceleration, RMS suspension travel, and RMS deflection are simulated and compared. The GA-PSO algorithm offers the biggest improvement in the amount of ride comfort, road holding, and handling performance of the vehicle. The effect of the optimization method is validated by field tests. According to the comparison of the field test result, after optimization, the RMS values of the vertical weighted acceleration, suspension travel, and tire deflection are improved by 18.46, 21.95, and 21.34%, respectively. Although the acceleration still means extreme discomfort, the duration time is improved by 56.25%.

According to the test result, the performance of the off-road vehicle is fully improved by the multiobjective optimization methods. Compared to the performance improved percentage (5~15%) of passenger vehicles on class B and class C roads, the performance of the off-road vehicle on the class F road can be improved with a higher percentage (15.19~21.95%). The different optimization methods may lead to various suspension parameters and vehicle performance. More MOO methods should be used in this area to acquire a better solution.

For vehicles with passive suspension, additional working conditions can be taken into consideration to improve vehicle performance on different roads. This method can be further used in either semiactive or active suspension. The optimized suspension parameters can be adjusted in the corresponding condition to maintain a better ride comfort, road holding, and handling performance of the vehicle.

Data Availability

The data used to support the findings of this study are available from the corresponding author upon request.

Conflicts of Interest

The authors declare no conflicts of interest.

Acknowledgments

This study was funded by Innovative Research Team Development Program of Ministry of Education of China (IRT_17R83) and the 111 Project (B17034) of China. Hubei Emergency Industry Technology Research Institute Co., Ltd. and Hubei Public Security Department are greatly acknowledged.

References

[1] M. Liu, F. Gu, and Y. Zhang, "Ride comfort optimization of in-wheel-motor electric vehicles with in-wheel vibration absorbers," *Energies*, vol. 10, no. 10, p. 1647, 2017.

[2] S. Kanarachos, A. M. Dizqah, G. Chrysakis, and M. E. Fitzpatrick, "Optimal design of a quadratic parameter varying vehicle suspension system using contrast-based fruit fly optimisation," *Applied Soft Computing*, vol. 62, pp. 463–477, 2018.

[3] Z. Yang, "Simulation analysis and optimization of ride quality of in-wheel motor electric vehicle," *Advances in Mechanical Engineering*, vol. 10, no. 5, 2018.

[4] Z. Li, L. Zheng, Y. Ren, Y. Li, and Z. Xiong, "Multi-objective optimization of active suspension system in electric vehicle with In-Wheel-Motor against the negative electromechanical coupling effects," *Mechanical Systems and Signal Processing*, vol. 116, pp. 545–565, 2019.

[5] G. Papaioannou and D. Koulocheris, "Multi-objective optimization of semi-active suspensions using KEMOGA

algorithm," *Engineering Science and Technology, an International Journal*, vol. 22, no. 4, pp. 1035–1046, 2019.

[6] M. A. A. Abdelkareem, L. Xu, M. K. A. Ali et al., "Vibration energy harvesting in automotive suspension system: a detailed review," *Applied Energy*, vol. 229, pp. 672–699, 2018.

[7] M. A. A. Abdelkareem, "On-field measurements of the dissipated vibrational power of an SUV car traditional viscous shock absorber," in *Proceedings of the International Design Engineering Technical Conferences and Computers and Information in Engineering Conference*, August 2018.

[8] M. A. A. Abdelkareem, L. Xu, X. Guo et al., "Energy harvesting sensitivity analysis and assessment of the potential power and full car dynamics for different road modes," *Mechanical Systems and Signal Processing*, vol. 110, pp. 307–332, 2018.

[9] M. Trikande, V. Jagirdar, and M. Sujithkumar, "Evaluation of semi-active suspension control strategies for 8x8 armoured vehicle using stochastic road profile inputs," *IFAC Proceedings Volumes*, vol. 47, no. 1, pp. 941–948, 2014.

[10] R. Ghasemiazar and S. Azadi, "Sensitivity analysis and optimization of an off road car vibration performance using DOE and RSM methods," SAE International, Warrendale, PA, USA, SAE Technical Paper 2012-01-1186, 2012.

[11] S. Xiudong, Q. Linfang, and L. Shou cheng, "Optimization of suspension parameter under random and impact load," *Vibration Test and Diagnosis*, vol. 2, pp. 122–125+161, 2006.

[12] L. Zhao, Y. Yu, C. Zhou, and F. Yang, "Modelling and validation of a seat suspension with rubber spring for off-road vehicles," *Journal of Vibration and Control*, vol. 24, no. 18, pp. 4110–4121, 2018.

[13] U. Solomon and C. Padmanabhan, "Semi-active hydro-gas suspension system for a tracked vehicle," *Journal of Terramechanics*, vol. 48, no. 3, pp. 225–239, 2011.

[14] J. Zhang, X. Li, and D. Liu, "Mine car suspension parameter optimisation based on improved particle swarm optimisation and approximation model," *International Journal of Vehicle Design*, vol. 80, no. 1, pp. 23–40, 2019.

[15] J. Sun, "Control research of nonlinear vehicle suspension system based on road estimation," SAE International, Warrendale, PA, USA, SAE Technical Paper 2018-01-0553, 2018.

[16] M. Mahmoodi-Kaleibar, "Optimization of suspension system of off-road vehicle for vehicle performance improvement," *Journal of Central South University*, vol. 20, no. 4, pp. 902–910, 2013.

[17] B. Lacroix, P. Seers, and Z. Liu, "A passive nonlinear damping design for a road race car application," SAE International, Warrendale, PA, USA, SAE Technical Paper 2006-01-1984, 2006.

[18] D. Özcan, "Optimization of nonlinear spring and damper characteristics for vehicle ride and handling improvement," SAE International, Warrendale, PA, USA, SAE Technical Paper 2008-01-2669, 2008.

[19] M. A. Abdelkareem, M. M. Makrahy, A. M. Abd-El-Tawwab, A. EL-Razaz, M. Kamal Ahmed Ali, and M. Moheyeldein, "An analytical study of the performance indices of articulated truck semi-trailer during three different cases to improve the driver comfort," *in Proceedings of the Institution of Mechanical Engineers, Part K: Journal of Multi-Body Dynamics*, vol. 232, no. 1, pp. 84–102, 2018.

[20] S. Gupta and C. S. Manohar, "An improved response surface method for the determination of failure probability and importance measures," *Structural Safety*, vol. 26, no. 2, pp. 123–139, 2004.

[21] I. Kaymaz and C. A. McMahon, "A response surface method based on weighted regression for structural reliability analysis," *Probabilistic Engineering Mechanics*, vol. 20, no. 1, pp. 11–17, 2005.

[22] N. Ghorbani, A. Kasaeian, A. Toopshekan, L. Bahrami, and A. Maghami, "Optimizing a hybrid wind-PV-battery system using GA-PSO and MOPSO for reducing cost and increasing reliability," *Energy*, vol. 154, pp. 581–591, 2018.

[23] L. Xu, Y. Jiang, and L. Wang, "Thermal decomposition of rape straw: pyrolysis modeling and kinetic study via particle swarm optimization," *Energy Conversion and Management*, vol. 146, pp. 124–133, 2017.

[24] H. Ahmed and J. Glasgow, "Swarm intelligence: concepts, models and applications," School of Computing, Queens University Technical Report, Queens University, Kingston, Canada, 2012.

[25] S. Mostaghim and Jürgen Teich, "Strategies for finding good local guides in multi-objective particle swarm optimization (MOPSO)," in *Proceedings of the 2003 IEEE Swarm Intelligence Symposium. SIS'03 (Cat. No. 03EX706)*, April 2003.

[26] B. Jamali, M. Rasekh, F. Jamadi, R. Gandomkar, and F. Makiabadi, "Using PSO-GA algorithm for training artificial neural network to forecast solar space heating system parameters," *Applied Thermal Engineering*, vol. 147, pp. 647–660, 2019.

[27] Y.-T. Kao and E. Zahara, "A hybrid genetic algorithm and particle swarm optimization for multimodal functions," *Applied Soft Computing*, vol. 8, no. 2, pp. 849–857, 2008.

[28] C. R. Houck, J. Joines, and M. G. Kay, "A genetic algorithm for function optimization: a Matlab implementation," *Ncsu-ie Tr*, vol. 95, no. 9, pp. 1–10, 1995.

[29] International Organization for Standardization, *Mechanical vibration and shock—evaluation of human exposure to whole body vibration—part1: general requirements*, International Organization for Standardization, Geneva, Switzerland, 1997.